J. Cent. South Univ. (2022) 29: 2467−2484
DOI: https://doi.org/10.1007/s11771-022-5106-6

Springer

Response of train-bridge system under intensive seismic excitation by random vibration method

WU Zhao-zhi(吴兆智), ZHANG Nan(张楠)*

School of Civil Engineering, Beijing Jiaotong University, Beijing 100044, China

Abstract: Earthquake is a kind of sudden and destructive random excitation in nature. It is significant to determine the probability distribution characteristics of the corresponding dynamic indicators to ensure the safety and the stability of structures when the intensive seismic excitation, the intensity of which is larger than 7, acts in train-bridge system. Firstly, the motion equations of a two-dimensional train-bridge system under the vertical random excitation of track irregularity and the vertical seismic acceleration are established, where the train subsystem is composed of 8 mutually independent vehicle elements with 48 degrees of freedom, while the single-span simple supported bridge subsystem is composed of 10 2D beam elements with 20 degrees of freedom on beam and 2 large mass degrees of freedom at the support. Secondly, Monte Carlo method and pseudo excitation method are adopted to analyze the statistical parameters of the system. The power spectrum density of random excitation is used to define a series of non-stationary pseudo excitation in pseudo excitation method and the trigonometric series of random vibration history samples in Monte Carlo method, respectively solved by precise integral method and Newmark-β method through the inter-system iterative procedure. Finally, the results are compared with the case under the weak seismic excitation, and show that the samples of vertical acceleration response of bridge and the offload factor of train obeys the normal distribution. In a high probability, the intensive earthquakes pose a greater threat to the safety and stability of bridges and trains than the weak ones.

Key words: random vibration method; intensive seismic excitation; train-bridge system; probability distribution; inter-system iteration; precise integral method

Cite this article as: WU Zhao-zhi, ZHANG Nan. Response of train-bridge system under intensive seismic excitation by random vibration method [J]. Journal of Central South University, 2022, 29(8): 2467−2484. DOI: https://doi.org/10.1007/s11771-022-5106-6.

1 Introduction

As the proportion of bridges in railway lines increases, the probability of trains running on the bridges during earthquakes is also increasing. Especially when the high-speed railway bridges face an intensive earthquake at a seismic intensity greater than 7, the bridge structure is damaged due to the violent vibration and the safety of passengers is seriously threatened [1]. Since the earthquake is a random load, if a single seismic acceleration sample is used to study this problem, it will bring some uncertainty to the calculation results. Therefore, the random vibration method is used to study and analyze the response of the train-bridge system (TBS) under the seismic excitation. The description of the relevant dynamic characteristic indicators from the perspective of probability distribution is of great significance to ensure the safety of train

Foundation item: Project(52178101) supported by the National Natural Science Foundation of China
Received date: 2021-07-02; **Accepted date:** 2022-03-13
Corresponding author: ZHANG Nan, PhD, Professor; E-mail: nzhang@bjtu.edu.cn; ORCID: https://orcid.org/0000-0003-0215-2465

operation and structural stability.

Nowadays, the research on the response of train-bridge system and the intensive earthquakes has got the attention of the scholars in China and abroad. YAU [2−3] studied the dynamic response of a suspension bridge subjected to moving loads and vertical earthquake action. NISHIMURA et al [4−5] performed theoretical analysis and experimental studies on the derailment mechanism and the running safety of high speed railway (HSR) vehicles subjected to earthquake and track irregularity. HE et al [6] developed an analytical approach to evaluate the influence of dynamic train-bridge interaction on the seismic response of the Shinkansen viaduct in Japan under moderate earthquakes and found that the response of bridge subsystem might be underestimated if the train load acted on the bridge only as additional mass. LOH et al [7] assessed seismic response characteristics of the bridge from both weak and strong ground excitations showing that weak and strong ground excitation will induce significant differences on the dynamic response of the bridge. QI et al [8] carried out the low reversed cyclic loading tests of composite frame system and studied the seismic behaviors of composite frames such as failure mode, hysteresis curve, strength degradation, rigidity degradation, ductility, and energy dissipation. ZHU et al [9] conducted a systematic study on the effect of heavy-haul trains on bridge seismic response and found that the peak moment of the main girder and peak stress of stay cables would tremendously increase during the earthquake.

With the application of random vibration method, the research on the response of train-bridge system is precisely conducted and statistically significant in China and abroad. LIN et al [10] set a simple and accurate algorithm for non-stationary responses of structures subjected to evolutionary random seismic excitation, which is an extension of pseudo excitation method (PEM) for stationary random seismic responses. ZHANG et al [11] modeled the bridge as an elastic Bernoulli-Euler beam and applied PEM to transform the random surface roughness into the superposition of a series of deterministic pseudo harmonic surface unevenness to simplify the solution of the non-stationary random vibration equations. HE et al solved the motion equation of vehicle-bridge coupled system through precise integral method (PIM) [12], and calculated the bridge response evolutionary power spectrum density (EPSD) from the bridge transient pseudo response, so as to deduce the standard deviation time history curve reflecting the response probability and statistical characteristics. ZHU et al [13] improved the efficiency of PEM by incorporating the self-adaptive Gauss integration (SGI) technology as a new combining integration and analyzed the random characteristics for the vehicle-bridge vibrations for different speeds and rail irregularities. YU et al [14] presented a new efficient computational framework, explicit time-domain method (ETDM), for non-stationary random vibration analysis of the vehicle-bridge system subjected to random track irregularity excitation and validated the accuracy and efficiency of the proposed method by the solutions obtained using the Monte Carlo method (MCM) and PEM.

Despite a large amount of research on TBS, earthquake and random vibration method, it is still lack of a comprehensive analysis of the TBS subjected to the intensive seismic excitation at the aspect of random and statistical characteristics. The article aims to determine the probability distribution characteristics of the acceleration response of bridge and the offload factor of train to ensure the safety and the stability of structures when the intensive seismic excitation acts on TBS.

By constructing a 2D TBS motion equation, considering the random excitation of track irregularity and the deterministic axle load excitation, the random excitation of seismic acceleration is input by large-mass method. Under the condition of the train running at a constant speed, the power spectrum density (PSD) of random excitation is used to define a series of non-stationary pseudo excitation in PEM and the trigonometric series of random vibration history samples in MCM, respectively solved by PIM and Newmark-β method (NβM) through inter-system iterative procedure. Finally, the results are compared with the case under weak seismic excitation and relevant suggestions are provided for ensuring the safety and the stability of the train operation and the bridge structure.

2 Establishment of 2D TBS motion equations

2.1 Motion equation of train subsystem

The train subsystem is composed of 8 same mutually independent vehicle elements. Each of them consists of a car-body, two bogies, four wheel-sets, and a two-layer spring-damper suspension system. To simplify the analysis while with enough accuracy, the assumptions are made as follows [15]:

1) The interaction does not exist among vehicle elements.

2) The car-body, bogies, and wheel-sets in each vehicle element are rigid.

3) The springs in vehicle element are linear, and the dampers are viscous.

4) The vehicle element is a linear system, namely the mass, damping, and stiffness matrices of the vehicle element are constant.

5) The train runs on the bridge at a constant speed.

6) Wheels and rails fit snugly. There is no sliding, climbing or derailment of the train on the rail.

With the assumptions above, each vehicle element is modeled with 6 independent degrees of freedom (DOFs) for the car-body and bogies, and with 4 dependent DOFs for the wheel-sets coupled by the vertical motion states of 4 contact points. The DOFs of each vehicle element are listed in Table 1 corresponding to Figure 1. z is the vertical displacement; φ is the pitch torsional displacement. The numbers of the bogies and the wheel-sets represent the front and rear orders. Subscript i denotes the number of certain vehicle element and equals 1, 2, 3, ⋯, 8.

Table 1 DOF parameters of a vehicle element

Vehicle element	DOF
Car-body	2 DOFs: z_{ci}, φ_{ci}
Bogies	4 DOFs: z_{b1i}, φ_{b1i}, z_{b2i}, φ_{b2i}
Wheel-sets	4 DOFs: z_{w1i}, z_{w2i}, z_{w3i}, z_{w4i}

In Figure 1(a), l_v, d_1 and d_2 represent respectively the length of a vehicle element, the half-length between two wheel-sets in a bogie and between two bogies in a car-body. The primary suspension system between the bogie and each wheel-set is characterized by springs with the spring coefficient k_1 and the viscous dampers with the damping coefficient c_1, while k_2 and c_2 for the second suspension system. m_c and I_c denote respectively car-body mass and the pitch moment of inertia. Accordingly, m_b and I_b are for the bogies. According to the D'Alembert principle, the motion equation of the train can be expressed as:

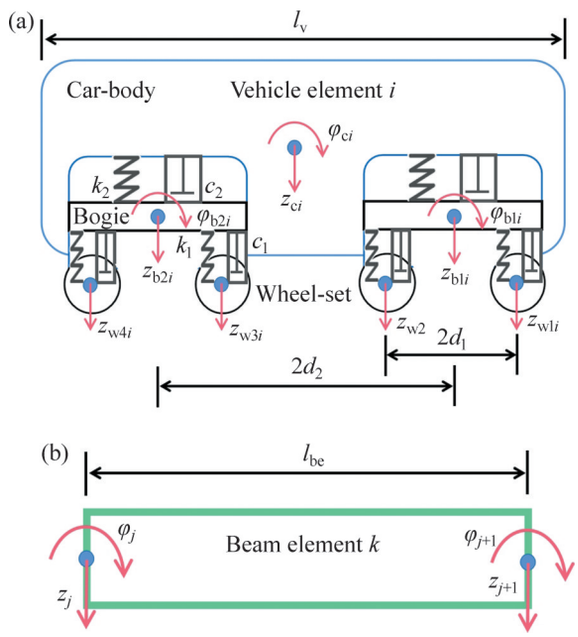

Figure 1 2D model of the vehicle element and the beam element: (a) Vehicle element i; (b) Beam element j

$$\boldsymbol{M}_t\ddot{\boldsymbol{u}}_t+\boldsymbol{C}_t\dot{\boldsymbol{u}}_t+\boldsymbol{K}_t\boldsymbol{u}_t=\boldsymbol{T}_t(k_1\boldsymbol{z}_w+c_1\dot{\boldsymbol{z}}_w) \tag{1}$$

where $\boldsymbol{M}_t$, $\boldsymbol{C}_t$, $\boldsymbol{K}_t$ and $\boldsymbol{T}_t$, are respectively the mass, the damping, the stiffness and projector matrices of the train and can be diagonally assembled of $\boldsymbol{M}_{ve}$, $\boldsymbol{C}_{ve}$, $\boldsymbol{K}_{ve}$ and $\boldsymbol{T}_{ve}$ of vehicle elements as Eq. (5). The expression of $\boldsymbol{C}_{ve}$, which is similar to Eq. (3), can be obtained simply by replacing the spring factors k with the corresponding damping factors c.

$$\boldsymbol{M}_{ve}=\mathrm{diag}\left[m_c \quad I_c \quad m_b \quad I_b \quad m_b \quad I_b\right] \tag{2}$$

$$\boldsymbol{K}_{ve}=\begin{bmatrix} 2k_2 & 0 & -k_2 & 0 & -k_2 & 0 \\ 0 & 2k_2d_2^2 & -k_2d_2 & 0 & k_2d_2 & 0 \\ -k_2 & -k_2d_2 & 2k_1+k_2 & 0 & 0 & 0 \\ 0 & 0 & 0 & 2k_1d_1^2 & 0 & 0 \\ -k_2 & k_2d_2 & 0 & 0 & 2k_1+k_2 & 0 \\ 0 & 0 & 0 & 0 & 0 & 2k_1d_1^2 \end{bmatrix} \tag{3}$$

$$\boldsymbol{T}_{\mathrm{ve}}=\begin{bmatrix}0&0&1&d_1&0&0\\0&0&1&-d_1&0&0\\0&0&0&0&1&d_1\\0&0&0&0&1&-d_1\end{bmatrix}^{\mathrm{T}} \tag{4}$$

$$\boldsymbol{M}_{\mathrm{t}}=\mathrm{diag}\left[\boldsymbol{M}_{\mathrm{ve}}\quad \boldsymbol{M}_{\mathrm{ve}}\quad \cdots\quad \boldsymbol{M}_{\mathrm{ve}}\right] \tag{5}$$

2.2 Motion equation of bridge subsystem

Composed of 10 mutually coupled plane beam elements, the bridge subsystem has a single-span constrained by the simple support. When a train runs on the bridge, the forces from the wheels are transmitted to the bridge structure through the track. In studying vertical vibrations of the train-bridge system, the bridge is usually analyzed with finite element method (FEM), using the following assumptions [16]:

1) The relative displacement between the track and the bridge deck, and the elastic effect of the track system is neglected.

2) The deformation of cross section in vibration is neglected for the beam with solid sections.

3) Bernoulli-Euler beam elements are adopted.

4) The Rayleigh damping is considered.

From above, each beam element is modeled as Figure 1(b) and the corresponding DOFs of each beam element are listed in Table 2. z is the vertical displacement; φ is the pitch torsional displacement along z axle. Subscript j denotes the number of certain beam element and equals 1, 2, 3, ⋯, 10.

Table 2 DOF parameters of a beam element

Beam element	DOF
Left node	2 DOFs: z_j, φ_j
Right node	2 DOFs: z_{j+1}, φ_{j+1}

l_{be}, E, I, S and ρ, represent respectively the length, elastic modulus, cross-sectional moment of inertia, cross-sectional area and density of a beam element. According to the D'Alembert principle, the motion equations of the bridge subsystem can be expressed as:

$$\begin{bmatrix}\boldsymbol{M}_{\mathrm{b}}&\boldsymbol{M}_{\mathrm{bp}}\\\boldsymbol{M}_{\mathrm{pb}}&\boldsymbol{M}_{\mathrm{p}}+\boldsymbol{M}_{\mathrm{L}}\end{bmatrix}\begin{pmatrix}\ddot{\boldsymbol{u}}_{\mathrm{b}}\\\ddot{\boldsymbol{u}}_{\mathrm{p}}\end{pmatrix}+\begin{bmatrix}\boldsymbol{C}_{\mathrm{b}}&\boldsymbol{C}_{\mathrm{bp}}\\\boldsymbol{C}_{\mathrm{pb}}&\boldsymbol{C}_{\mathrm{p}}\end{bmatrix}\begin{pmatrix}\dot{\boldsymbol{u}}_{\mathrm{b}}\\\dot{\boldsymbol{u}}_{\mathrm{p}}\end{pmatrix}+\begin{bmatrix}\boldsymbol{K}_{\mathrm{b}}&\boldsymbol{K}_{\mathrm{bp}}\\\boldsymbol{K}_{\mathrm{pb}}&\boldsymbol{K}_{\mathrm{p}}\end{bmatrix}\begin{pmatrix}\boldsymbol{u}_{\mathrm{b}}\\\boldsymbol{u}_{\mathrm{p}}\end{pmatrix}=\begin{pmatrix}\boldsymbol{T}_{\mathrm{b}}\boldsymbol{f}_{\mathrm{r}}\\(\boldsymbol{M}_{\mathrm{p}}+\boldsymbol{M}_{\mathrm{L}})\ddot{\boldsymbol{u}}_{\mathrm{p}}\end{pmatrix} \tag{6}$$

The mass matrix $\boldsymbol{M}_{\mathrm{b}}$ and stiffness matrix $\boldsymbol{K}_{\mathrm{b}}$ of the bridge can be formed by withdrawing the non-support elements from the matrix $\boldsymbol{K}_{\mathrm{be10}}$ and $\boldsymbol{M}_{\mathrm{be10}}$ assembled in the way of Eqs. (9) and (10) of the mass and stiffness matrices of beam elements, $\boldsymbol{M}_{\mathrm{be}}$ and $\boldsymbol{K}_{\mathrm{be}}$. Also, $\boldsymbol{0}$ and $\boldsymbol{I}$ respectively represents zero matrix and identical matrix.

$$\boldsymbol{K}_{\mathrm{be}}=\frac{EI}{l_{\mathrm{be}}^3}\begin{bmatrix}12&6l_{\mathrm{be}}&-12&6l_{\mathrm{be}}\\6l_{\mathrm{be}}&4l_{\mathrm{be}}^2&-6l_{\mathrm{be}}&2l_{\mathrm{be}}^2\\-12&-6l_{\mathrm{be}}&12&-6l_{\mathrm{be}}\\6l_{\mathrm{be}}&2l_{\mathrm{be}}^2&-6l_{\mathrm{be}}&4l_{\mathrm{be}}^2\end{bmatrix} \tag{7}$$

$$\boldsymbol{M}_{\mathrm{be}}=\frac{\rho Sl_{\mathrm{be}}}{420}\begin{bmatrix}156&22l_{\mathrm{be}}&54&-13l_{\mathrm{be}}\\22l_{\mathrm{be}}&4l_{\mathrm{be}}^2&13l_{\mathrm{be}}&-3l_{\mathrm{be}}^2\\54&13l_{\mathrm{be}}&156&-22l_{\mathrm{be}}\\-13l_{\mathrm{be}}&-3l_{\mathrm{be}}^2&-22l_{\mathrm{be}}&4l_{\mathrm{be}}^2\end{bmatrix} \tag{8}$$

$$\boldsymbol{K}_{\mathrm{be10}}=\left[\boldsymbol{0}_{4\times(2j-2)}\quad \boldsymbol{I}_{4\times4}\quad \boldsymbol{0}_{4\times(20-2j)}\right]^{\mathrm{T}}\cdot \boldsymbol{K}_{\mathrm{be}}\left[\boldsymbol{0}_{4\times(2j-2)}\quad \boldsymbol{I}_{4\times4}\quad \boldsymbol{0}_{4\times(20-2j)}\right] \tag{9}$$

$$\boldsymbol{M}_{\mathrm{be10}}=\left[\boldsymbol{0}_{4\times(2j-2)}\quad \boldsymbol{I}_{4\times4}\quad \boldsymbol{0}_{4\times(20-2j)}\right]^{\mathrm{T}}\cdot \boldsymbol{M}_{\mathrm{be}}\left[\boldsymbol{0}_{4\times(2j-2)}\quad \boldsymbol{I}_{4\times4}\quad \boldsymbol{0}_{4\times(20-2j)}\right] \tag{10}$$

$$\boldsymbol{K}_{\mathrm{b}}=\frac{EI}{l_{\mathrm{be}}^3}\begin{bmatrix}24&0&-12&6l_{\mathrm{be}}&&&&&&\\0&8l_{\mathrm{be}}^2&-6l_{\mathrm{be}}&2l_{\mathrm{be}}^2&&&&&&\\-12&-6l_{\mathrm{be}}&24&0&-12&6l_{\mathrm{be}}&&&&\\6l_{\mathrm{be}}&2l_{\mathrm{be}}^2&0&8l_{\mathrm{be}}^2&-6l_{\mathrm{be}}&2l_{\mathrm{be}}^2&&&&\\&&-12&-6l_{\mathrm{be}}&24&0&&&&\\&&6l_{\mathrm{be}}&2l_{\mathrm{be}}^2&0&8l_{\mathrm{be}}^2&&&&\\&&&&&&\ddots&&&\\&&&&&&&24&0&-12&6l_{\mathrm{be}}\\&&&&&&&0&8l_{\mathrm{be}}^2&-6l_{\mathrm{be}}&2l_{\mathrm{be}}^2\\&&&&&&&-12&-6l_{\mathrm{be}}&24&0\\&&&&&&&6l_{\mathrm{be}}&2l_{\mathrm{be}}^2&0&8l_{\mathrm{be}}^2\end{bmatrix}_{18\times18} \tag{11}$$

$$\boldsymbol{M}_{\mathrm{b}}=\frac{\rho Sl_{\mathrm{be}}}{420}\begin{bmatrix}312&0&54&-13l_{\mathrm{be}}&&&&&&\\0&8l_{\mathrm{be}}^2&13l_{\mathrm{be}}&-3l_{\mathrm{be}}^2&&&&&&\\54&13l_{\mathrm{be}}&312&0&54&-13l_{\mathrm{be}}&&&&\\-13l_{\mathrm{be}}&-3l_{\mathrm{be}}^2&0&8l_{\mathrm{be}}^2&13l_{\mathrm{be}}&-3l_{\mathrm{be}}^2&&&&\\&&54&13l_{\mathrm{be}}&312&0&&&&\\&&-13l_{\mathrm{be}}&-3l_{\mathrm{be}}^2&0&8l_{\mathrm{be}}^2&&&&\\&&&&&&\ddots&&&\\&&&&&&&312&0&54&-13l_{\mathrm{be}}\\&&&&&&&0&8l_{\mathrm{be}}^2&13l_{\mathrm{be}}&-3l_{\mathrm{be}}^2\\&&&&&&&54&13l_{\mathrm{be}}&312&0\\&&&&&&&-13l_{\mathrm{be}}&-3l_{\mathrm{be}}^2&0&8l_{\mathrm{be}}^2\end{bmatrix}_{18\times18} \tag{12}$$

The mass matrix $\boldsymbol{M}_{\mathrm{p}}$ and stiffness matrices $\boldsymbol{K}_{\mathrm{p}}$ of support can be formed in Eqs. (14) by withdrawing the vertical DOF elements of support from the matrix $\boldsymbol{K}_{\mathrm{be10}}$ and $\boldsymbol{M}_{\mathrm{be10}}$. In Eqs. (15) and (16), the remained elements are used to form the bridge-support coupling matrix of stiffness and mass, $\boldsymbol{K}_{\mathrm{bp}}$ and $\boldsymbol{M}_{\mathrm{bp}}$. $\boldsymbol{K}_{\mathrm{bp}}$ and $\boldsymbol{M}_{\mathrm{bp}}$ are respectively the transpose of $\boldsymbol{K}_{\mathrm{bp}}$ and $\boldsymbol{M}_{\mathrm{bp}}$.

$$\boldsymbol{K}_{\mathrm{p}}=\frac{EI}{l_{\mathrm{be}}^3}\begin{bmatrix}12 & 6l_{\mathrm{be}} & 0 & 0\\ 6l_{\mathrm{be}} & 4l_{\mathrm{be}}^2 & 0 & 0\\ 0 & 0 & 12 & -6l_{\mathrm{be}}\\ 0 & 0 & -6l_{\mathrm{be}} & 4l_{\mathrm{be}}^2\end{bmatrix} \tag{13}$$

$$\boldsymbol{M}_{\mathrm{p}}+\boldsymbol{M}_{\mathrm{L}}=\frac{\rho Sl_{\mathrm{be}}}{420}\begin{bmatrix}156+m_{\mathrm{L}} & 22l_{\mathrm{be}} & 0 & 0\\ 22l_{\mathrm{be}} & 4l_{\mathrm{be}}^2 & 0 & 0\\ 0 & 0 & 156+m_{\mathrm{L}} & -22l_{\mathrm{be}}\\ 0 & 0 & -22l_{\mathrm{be}} & 4l_{\mathrm{be}}^2\end{bmatrix} \tag{14}$$

$$\boldsymbol{K}_{\mathrm{bp}}=\boldsymbol{K}_{\mathrm{pb}}^{\mathrm{T}}=\frac{EI}{l_{\mathrm{be}}^3}\begin{bmatrix}-12 & -6l_{\mathrm{be}} & 0 & 0\\ 6l_{\mathrm{be}} & 2l_{\mathrm{be}}^2 & \vdots & \vdots\\ 0 & 0 & 0 & 0\\ \vdots & \vdots & -12 & 6l_{\mathrm{be}}\\ 0 & 0 & -6l_{\mathrm{be}} & 2l_{\mathrm{be}}^2\end{bmatrix}_{18\times 4} \tag{15}$$

$$\boldsymbol{M}_{\mathrm{bp}}=\boldsymbol{M}_{\mathrm{pb}}^{\mathrm{T}}=\frac{\rho Sl_{\mathrm{be}}}{420}\begin{bmatrix}54 & 13l_{\mathrm{be}} & 0 & 0\\ -13l_{\mathrm{be}} & -3l_{\mathrm{be}}^2 & \vdots & \vdots\\ 0 & 0 & 0 & 0\\ \vdots & \vdots & 54 & -13l_{\mathrm{be}}\\ 0 & 0 & 13l_{\mathrm{be}} & -3l_{\mathrm{be}}^2\end{bmatrix}_{18\times 4} \tag{16}$$

In order to apply seismic acceleration to the bridge supports, large mass $\boldsymbol{M}_{\mathrm{L}}$ should be added on the diagonal elements corresponding to the supports in the mass matrix $\boldsymbol{M}_{\mathrm{p}}$ on the left side of the motion equation, and meanwhile, the external load should be applied to the elements corresponding to the supports in the force vector on the right side of the equation. The values of the external load are equal to the product of the seismic acceleration and the sum of the large mass and the diagonal elements. In Eq. (14), m_{L} is the large mass, which is usually 10^3–10^6 times the total mass of the bridge.

Based on assumption (4), the damping matrix $\boldsymbol{C}_{\mathrm{b}}$ of the bridge can be expressed in Eq. (17) by combination of $\boldsymbol{M}_{\mathrm{b}}$ and $\boldsymbol{K}_{\mathrm{b}}$ with ξ, damping ratio of the bridge, and ω_1 and ω_2, respectively the first and second order angular frequencies of the bridge.

$$\boldsymbol{C}_{\mathrm{b}}=\frac{2\xi\omega_1\omega_2}{\omega_1+\omega_2}\boldsymbol{M}_{\mathrm{b}}+\frac{2\xi}{\omega_1+\omega_2}\boldsymbol{K}_{\mathrm{b}} \tag{17}$$

$\boldsymbol{f}_{\mathrm{r}}$ is the wheel-rail force vector and can be expressed as a linear addition of the car body-bogie feedback response, the wheel-set motion state, and the axle load as in Eq. (18).

$$\boldsymbol{f}_{\mathrm{r}}=-m_{\mathrm{w}}\ddot{\boldsymbol{z}}_{\mathrm{w}}+c_1[\boldsymbol{T}_{\mathrm{t}}^{\mathrm{T}}\dot{\boldsymbol{u}}_{\mathrm{t}}-\dot{\boldsymbol{z}}_{\mathrm{w}}]+k_1[\boldsymbol{T}_{\mathrm{t}}^{\mathrm{T}}\boldsymbol{u}_{\mathrm{t}}-\boldsymbol{z}_{\mathrm{w}}]+\left(m_{\mathrm{w}}+\frac{m_{\mathrm{b}}}{2}+\frac{m_{\mathrm{c}}}{4}\right)g \tag{18}$$

$\boldsymbol{T}_{\mathrm{b}}$ in Eq. (19) is the projector matrix of bridge to project $\boldsymbol{f}_{\mathrm{r}}$ to the nodes of the beam elements contacted by the wheel-sets. As sub-matrix, $\boldsymbol{T}_{\mathrm{b}}^{\mathrm{ve}}$ in $\boldsymbol{T}_{\mathrm{b}}$ can be sequenced as sub-vectors $\boldsymbol{\tau}_{\mathrm{b}}^{\mathrm{w}}$ for 4 wheel-sets in a vehicle element. Because of the time difference among 4 wheel-sets in a vehicle element, $\boldsymbol{\tau}_{\mathrm{b}}^{\mathrm{w}}$ can be differed in Eq. (20) by subtraction of time delay and in Eq. (21), adopts the sub-function P projecting the wheel-rail force respectively to the vertical DOF in Eq. (22) and to the pitch torsional DOF in Eq. (23).

$$\boldsymbol{T}_{\mathrm{b}}=\left[\boldsymbol{T}_{\mathrm{b}}^{\mathrm{ve}}(t)\quad \boldsymbol{T}_{\mathrm{b}}^{\mathrm{ve}}\left(t-\tfrac{l_{\mathrm{v}}}{V}\right)\quad \boldsymbol{T}_{\mathrm{b}}^{\mathrm{ve}}\left(t-\tfrac{2l_{\mathrm{v}}}{V}\right)\quad \cdots\quad \boldsymbol{T}_{\mathrm{b}}^{\mathrm{ve}}\left(t-\tfrac{7l_{\mathrm{v}}}{V}\right)\right] \tag{19}$$

$$\boldsymbol{T}_{\mathrm{b}}^{\mathrm{ve}}=\left[\boldsymbol{\tau}_{\mathrm{b}}^{\mathrm{w}}(t)\quad \boldsymbol{\tau}_{\mathrm{b}}^{\mathrm{w}}\left(t-\tfrac{2d_1}{V}\right)\quad \boldsymbol{\tau}_{\mathrm{b}}^{\mathrm{w}}\left(t-\tfrac{2d_2}{V}\right)\quad \boldsymbol{\tau}_{\mathrm{b}}^{\mathrm{w}}\left(t-\tfrac{2(d_1+d_2)}{V}\right)\right] \tag{20}$$

$$\boldsymbol{\tau}_{\mathrm{b}}^{\mathrm{w}}(t)=\left[P_z(t)\quad P_\phi(t)\quad P_z\left(t-\tfrac{l_{\mathrm{be}}}{V}\right)\quad P_\phi\left(t-\tfrac{l_{\mathrm{be}}}{V}\right)\quad \cdots\quad P_z\left(t-\tfrac{10l_{\mathrm{be}}}{V}\right)\quad P_\phi\left(t-\tfrac{10l_{\mathrm{be}}}{V}\right)\right]^{\mathrm{T}} \tag{21}$$

$$P_z(t)=\begin{cases}0, & t\le t_0\\ \dfrac{3\left[V(t-t_0)\right]^2}{l_{\mathrm{be}}^2}-\dfrac{2\left[V(t-t_0)\right]^3}{l_{\mathrm{be}}^3}, & t_0<t\le\frac{l_{\mathrm{be}}}{V}+t_0\\ 1-\dfrac{3\left[V(t-t_0-\frac{l_{\mathrm{be}}}{V})\right]^2}{l_{\mathrm{be}}^2}+\dfrac{2\left[V(t-t_0-\frac{l_{\mathrm{be}}}{V})\right]^3}{l_{\mathrm{be}}^3}, & \\ \qquad \frac{l_{\mathrm{be}}}{V}+t_0<t\le\frac{2l_{\mathrm{be}}}{V}+t_0\\ 0, & t>\frac{2l_{\mathrm{be}}}{V}+t_0\end{cases} \tag{22}$$

$$P_\phi(t)=\begin{cases}0, & t\le t_0\\ -\dfrac{\left[V(t-t_0)\right]^2}{l_{\mathrm{be}}}+\dfrac{\left[V(t-t_0)\right]^3}{l_{\mathrm{be}}^2}, & t_0\le t<\frac{l_{\mathrm{be}}}{V}+t_0\\ V(t-t_0-\frac{l_{\mathrm{be}}}{V})-\dfrac{2\left[V(t-t_0-\frac{l_{\mathrm{be}}}{V})\right]^2}{l_{\mathrm{be}}}+ & \\ \qquad \dfrac{\left[V(t-t_0-\frac{l_{\mathrm{be}}}{V})\right]^3}{l_{\mathrm{be}}^2}, & \frac{l_{\mathrm{be}}}{V}+t_0<t\le\frac{2l_{\mathrm{be}}}{V}+t_0\\ 0, & t>\frac{2l_{\mathrm{be}}}{V}+t_0\end{cases} \tag{23}$$

3 Analysis and solution of TBS based on random vibration method

3.1 Random excitation sampling and solution based on MCM-NβM

MCM is named after the famous casino in Monaco. It is a method for setting a random process, repeatedly generating a time series, calculating parameter estimates and statistics, and then studying its distribution characteristics [17].

As to simplify the analysis while with enough accuracy, relevant assumptions are made as follows:

1) Seismic acceleration time history is a uniformly modulated non-stationary Gaussian random process.

2) The influence from spatial variation of seismic ground motion is excluded.

Based on the assumptions above, the seismic acceleration is input to the vertical DOFs consistently of the support. The original signal samples can be generated by the trigonometric series superposition method, and the modulation function can be selected from the Bogdanoff-Goldberg-Bernard single exponential model [18], as shown in Eq. (24).

$$\ddot{\boldsymbol{u}}_{\mathrm{p}}(t)=1.36t\mathrm{e}^{-0.5t}\sqrt{2}\sum_{k=1}^{N_1}\sqrt{S_{\mathrm{e}}(\omega_k)\mathrm{d}\omega_k}\cdot \cos[\omega_k t+\varphi_k]\begin{bmatrix}1\\0\\1\\0\end{bmatrix} \tag{24}$$

where S_{e} is the given seismic acceleration PSD; ω_{k} is an angular frequency sample; dω is the bandwidth; and φ_k is a random phase angle obeying the uniform distribution $U(0, 2\pi)$. The integer order of k ranges from 1 to N_1.

A similar method can be used for the time history sampling of track irregularities. The track irregularity is regarded as a stationary Gaussian random process, and in Eq. (25), the wheel-set displacement can be expressed as the sum of the bridge displacement and the track irregularity at the wheel-rail contact point. As to the wheel-set running outside the deck, its displacement should include the seismic displacement by the quadratic integration of the seismic acceleration.

$$\boldsymbol{z}_{\mathrm{w}}(t)=\boldsymbol{T}_{\mathrm{b}}^{\mathrm{T}}\boldsymbol{u}_{\mathrm{b}}+\begin{bmatrix}1&0&0&0\end{bmatrix}\iint\ddot{\boldsymbol{u}}_{\mathrm{p}}(t)\mathrm{d}t+\sqrt{2}\sum_{k=1}^{N_2}\sqrt{S_{\mathrm{v}}(n_k)\mathrm{d}n_k}\cos(n_k v(t-t_0)+\theta_k) \tag{25}$$

where S_{v} is the given vertical track irregularity PSD, n_k is an angular wave number sample, dn is the bandwidth, and θ_k is a random phase angle obeying the uniform distribution $U(0, 2\pi)$. The integer order of k ranges from 1 to N_2.

After the sampling, different series of system response subjected to different random excitation samples can be solved by NβM, thus reflecting that the MCM is essentially a random sampling method.

3.2 Establishment and solution of random excitation based on PEM-PIM

In PEM, with the given random excitation PSD, a series of input pseudo simple harmonic excitation are constructed, converting the calculation of non-stationary random vibration into stepwise precise integral calculation, to obtain the structural response power spectrum and the variance [19].

Based on the same assumptions as last section, there is no phase difference between the input points. The pseudo seismic acceleration can be expressed in Eq. (26). The overhead tildes represent the variables in the pseudo form as the function of angular frequency ω and time t. Bogdanoff-Goldberg-Bernard single exponential model, a kind of time-derivable slow-varying uniform modulation function, are adopted to construct the non-stationary pseudo excitation through variable separation.

$$\ddot{\tilde{\boldsymbol{u}}}_{\mathrm{p}}(\omega,\ t)=1.36t\mathrm{e}^{-0.5t}\sqrt{S_{\mathrm{e}}(\omega)}\ \mathrm{e}^{\mathrm{j}\omega t}\begin{bmatrix}1\\0\\1\\0\end{bmatrix} \tag{26}$$

In PEM, the pseudo wheel-set displacement should be separately defined as for the track irregularity and the seismic excitation because they are two different types of independent random excitation and only their PSD are allowed to be superposed linearly. Firstly, in Eq. (27), PSD of track irregularity in angular frequency and wave number domain is used to structure pseudo wheel-set displacement $\tilde{\boldsymbol{z}}_{\mathrm{w}}$, where $\boldsymbol{p}$ is the matrix containing the phase difference among 32 wheel-sets of a train with 8 vehicles and sequenced in the

way of Eqs. (28) and (29). Secondly, as to the seismic excitation, the pseudo wheel-set displacement in Eq. (30) should include the pseudo seismic displacement by the quadratic integration of the pseudo seismic acceleration.

$$\tilde{\boldsymbol{z}}_{\mathrm{w}}=\boldsymbol{T}_{\mathrm{b}}^{\mathrm{T}}\tilde{\boldsymbol{u}}_{\mathrm{b}}+\sqrt{\frac{S_{\mathrm{v}}(n)}{V}}\,\mathrm{e}^{\mathrm{j}nVt}\boldsymbol{p}=\boldsymbol{T}_{\mathrm{b}}^{\mathrm{T}}\tilde{\boldsymbol{u}}_{\mathrm{b}}+\sqrt{S_{\mathrm{ir}}(\omega)}\,\mathrm{e}^{\mathrm{j}\omega t}\boldsymbol{p} \tag{27}$$

$$\boldsymbol{p}=\begin{bmatrix}\boldsymbol{p}_1^{\mathrm{ve}} & \boldsymbol{p}_2^{\mathrm{ve}} & \boldsymbol{p}_3^{\mathrm{ve}} & \cdots & \boldsymbol{p}_8^{\mathrm{ve}}\end{bmatrix}^{\mathrm{T}} \tag{28}$$

$$\boldsymbol{p}_i^{\mathrm{ve}}=\begin{bmatrix}\mathrm{e}^{-\mathrm{j}\omega(i-1)\frac{l_{\mathrm{v}}}{V}} & \mathrm{e}^{-\mathrm{j}\omega[\frac{(i-1)l_{\mathrm{v}}+2d_1}{V}]} & \mathrm{e}^{-\mathrm{j}\omega[\frac{(i-1)l_{\mathrm{v}}+2d_2}{V}]} & \mathrm{e}^{-\mathrm{j}\omega[\frac{(i-1)l_{\mathrm{v}}+2d_1+2d_2}{V}]}\end{bmatrix} \tag{29}$$

$$\tilde{\mathbf{z}}_{\mathrm{w}}=\boldsymbol{T}_{\mathrm{b}}^{\mathrm{T}}\tilde{\boldsymbol{u}}_{\mathrm{b}}+\begin{bmatrix}1 & 0 & 0 & 0\end{bmatrix}\iint\tilde{\boldsymbol{u}}_{\mathrm{p}}\mathrm{d}t \tag{30}$$

As for the pseudo wheel-rail force, in PEM, its deterministic part is excluded and it can be presented as follows:

$$\tilde{\boldsymbol{f}}_{\mathrm{r}}=-m_{\mathrm{w}}\ddot{\tilde{\boldsymbol{z}}}_{\mathrm{w}}+c_1[\boldsymbol{T}_{\mathrm{t}}^{\mathrm{T}}\dot{\tilde{\boldsymbol{u}}}_{\mathrm{t}}-\dot{\tilde{\boldsymbol{z}}}_{\mathrm{w}}]+k_1[\boldsymbol{T}_{\mathrm{t}}^{\mathrm{T}}\tilde{\boldsymbol{u}}_{\mathrm{t}}-\tilde{\boldsymbol{z}}_{\mathrm{w}}] \tag{31}$$

PIM is an integral method proposed by ZHONG et al [20]. He expresses the motion equation of the structure in the Hamiltonian system, so that the accuracy of the solution can be improved. The state space equation of the system is established by reducing the order in Eq. (32) containing the pseudo force vector $\tilde{\boldsymbol{F}}$ within the pseudo state force vector $\tilde{\boldsymbol{r}}$.

$$\dot{\tilde{\boldsymbol{x}}}=\boldsymbol{H}\tilde{\boldsymbol{x}}+\tilde{\boldsymbol{r}},\qquad\tilde{\boldsymbol{r}}=\begin{bmatrix}\boldsymbol{0}\\ \tilde{\boldsymbol{F}}\end{bmatrix},\qquad\tilde{\boldsymbol{x}}_0=\begin{pmatrix}\tilde{\boldsymbol{u}}(\omega,\,0)\\ \dot{\tilde{\boldsymbol{u}}}(\omega,\,0)\end{pmatrix} \tag{32}$$

where $\tilde{\boldsymbol{x}}$ is the pseudo state vector, with the subscript 0 representing the initial condition, composed of the pseudo displacement and velocity, while $\boldsymbol{H}$ is the stationary state space matrix containing stiffness $\boldsymbol{K}$, mass $\boldsymbol{M}$ and damping $\boldsymbol{C}$ matrices of the system, and can be expressed as:

$$\boldsymbol{H}=\begin{bmatrix}\boldsymbol{0} & \boldsymbol{I}\\ -\boldsymbol{M}^{-1}\boldsymbol{K} & -\boldsymbol{M}^{-1}\boldsymbol{C}\end{bmatrix} \tag{33}$$

The theory of ordinary differential equations is applied. When integrating in the time domain, the response in the next step can be expressed as:

$$\boldsymbol{X}(\omega,\,t+\Delta t)=\mathrm{e}^{\boldsymbol{H}\cdot\Delta t}\boldsymbol{X}(\omega,\,t)+\int_t^{t+\Delta t}\mathrm{e}^{\boldsymbol{H}\cdot(t+\Delta t-\tau)}\tilde{\boldsymbol{r}}(\omega,\,\tau)\mathrm{d}\tau \tag{34}$$

Assuming that the excitation load is linear, the following relationship exists:

$$\tilde{\boldsymbol{r}}(\omega,\,\tau)=\tilde{\boldsymbol{r}}_0+\tilde{\boldsymbol{r}}_1\tau=\tilde{\boldsymbol{r}}(\omega,\,t)+\frac{\tilde{\boldsymbol{r}}(\omega,\,t+\Delta t)-\tilde{\boldsymbol{r}}(\omega,\,t)}{\Delta t}\tau \tag{35}$$

By substituting Eq. (35) into Eq. (34), the response by PIM is expressed as:

$$\tilde{\boldsymbol{x}}(\omega,\,t+\Delta t)=\mathrm{e}^{\boldsymbol{H}\cdot\Delta t}(\boldsymbol{X}(\omega,\,t)+\boldsymbol{H}^{-1}(\tilde{\boldsymbol{r}}_0+\boldsymbol{H}^{-1}\tilde{\boldsymbol{r}}_1))-\boldsymbol{H}^{-1}(\tilde{\boldsymbol{r}}_0+\boldsymbol{H}^{-1}\tilde{\boldsymbol{r}}_1+\Delta t\tilde{\boldsymbol{r}}_1) \tag{36}$$

3.3 Inter-system iteration procedures

The inter-system iteration method, also called as the whole-process iteration method, is a newly developed method to solve the TBS motion equation [22].

In this method shown in Figure 2, firstly, the vehicle motion and the wheel-rail force can be calculated through solution of independent train equations under the assumption that the bridge

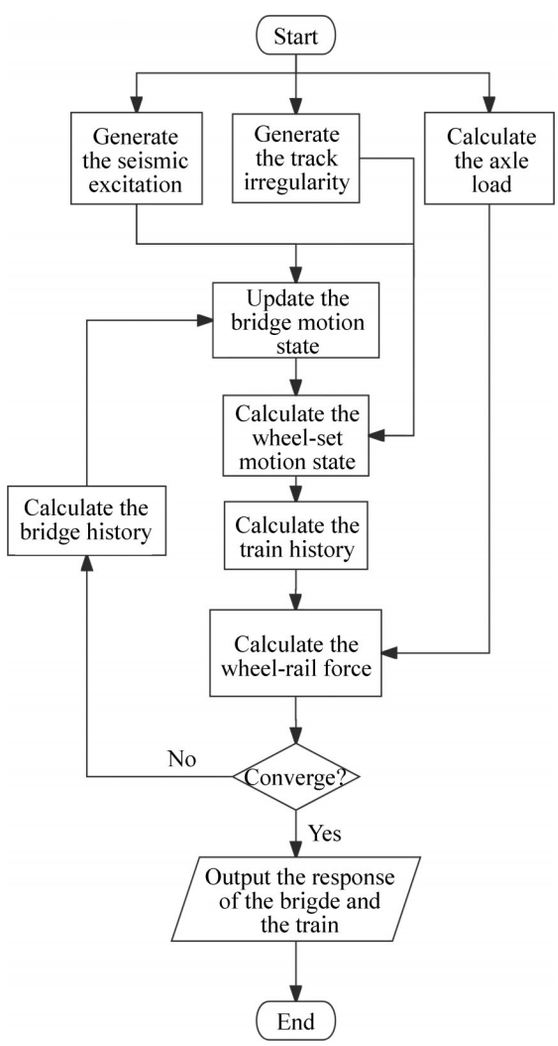

Figure 2 Flowchart of inter-system iteration procedure

subsystem is rigid, the wheel-rail forces and the seismic load are applied to the bridge, thus the motion state of the bridge can be calculated through the solution of the independent bridge equation. Secondly, the next iteration is carried out by the superposition of the calculated deck motion time histories with the track irregularities as an updated train subsystem excitation. The wheel-rail force can also be adopted as the index for the convergence judgment. When the absolute difference from the last iteration is smaller than 10 N, the procedure is judged to be convergent. Finally, the output will be implemented, followed by the end of the procedure.

The deterministic excitation like axle load history is simultaneously input with the random excitation history samples generated by MCM, including the track irregularity and the seismic excitation, into TBS and solved by NβM, which aims to obtain the history distribution and the tentative statistical parameters (expectation and variance) of the response, offload factors, etc.

By PEM, the deterministic excitation is excluded. The pseudo form of random excitation established by sampling the PSD is solved by PIM, which aims to obtain the theoretical variance and PSD of the response, offload factors, etc. In addition, the solutions to the TBS respectively subjected to the track irregularity and the seismic excitation should be separately conducted while the PSD by these two separate approaches should be superposed in the end.

Without any random excitation input, the solution by PIM to TBS only with the deterministic excitation input like axle load aims to obtain the theoretical expectation of the response, offload factors, etc.

3.4 Random dynamic characteristics of TBS under intensive seismic excitation

The vibration level of the bridge can be characterized by its vibration acceleration. The HSR code in China (TB 10621−2014) [21] stipulates that when the train crosses the bridge, the vertical acceleration limit of the ballast-less bridge deck under the intensive vibration frequency of 20 Hz is below 5 m/s^2.

Offload factor, the ratio of wheel load reduction at the offloaded side to the average load of the two wheel-sets, is used to check whether the vehicle will derail due to overlarge offload at one side of wheel-set [15]. For vehicles running on the bridge, the wheel load decreases when the wheel vibrates upside, which will, even with small or zero lateral wheel-rail force, induce derailment due to the relative lateral displacement between wheel and rail. Therefore, as a criterion for anti-derailment, offload factor has practical significance for vehicles running on the bridge. The HSR code in China (TB 10621−2014) [21] stipulates that the safe offload factor should be less than 0.6. The offload factor vector can be expressed in Eq. (37).

$$\boldsymbol{R}_{\mathrm{w}}=\frac{\boldsymbol{f}_{\mathrm{r}}}{\left(m_{\mathrm{w}}+\dfrac{m_{\mathrm{b}}}{2}+\dfrac{m_{\mathrm{c}}}{4}\right)g}-1 \tag{37}$$

In order to obtain the tentative possibility density function curve, which is smooth and continuous, Kernel estimation is adopted and can be defined as follows: Let (x_1, x_2, ⋯ , x_n) be n independent and identically distributed samples drawn from some uni-variate distribution at an instant with an unknown density p at any given function variable x [23]. Its non-stationary kernel density estimator is presented as:

$$p(x,\ t)=\frac{1}{nh}\sum_{i=1}^{n}K\left(\frac{x-x_i(t)}{h}\right) \tag{38}$$

where the domain of definition for x is within the real number set; $x_i(t)$ is the number i of the random samples in the time domain by MCM; K is a kernel function and h is a parameter of window governing the degree of smoothing of the estimation. In Eq. (39), K is often chosen as the density of a standard Gaussian function, and in Eq. (40), a popular way to obtain a value of h is to assume that the sample is distributed according to a Gaussian distribution law. $\sigma(t)$ is the non-stationary standard variance of the random history samples.

$$K(x)=\frac{1}{\sqrt{2\pi}}\exp\left(-\frac{1}{2}x^2\right) \tag{39}$$

$$h=1.06\sigma(t)n^{-1/5} \tag{40}$$

The goodness of fit (GOF) is used to verify whether the hypothetical probability distribution is valid or not [24], as in Eq. (41). The closer the goodness of fit is to 1, the more the experimental distribution meets the theoretical hypothesis. $p(x,\ t)$

is the experimental non-stationary probability density to fit the probability density of the theoretical normal distribution $f(x, t)$ and $p_m(t)$ is the non-stationary average calculated along the variable x for $p(x, t)$.

$$R^2(t)=1-\frac{\sum_{x\in R}(p(x,\ t)-f(x,\ t))^2}{\sum_{x\in R}(p(x,\ t)-p_m(t))^2} \tag{41}$$

The EPSD reflects the time varying of different components, and its matrix form can be obtained by multiplication of the conjugate and the transpose of the corresponding pseudo vectors. For example, the matrix of EPSD for the displacement response can be calculated in Eq. (42).

$$\boldsymbol{S}_{uu}(\omega,t)=\tilde{\boldsymbol{u}}^*\tilde{\boldsymbol{u}}^{\mathrm{T}} \tag{42}$$

The track irregularity and the seismic excitation are assumed to be random excitation with the zero mean value. Hence, after applying the square root on the integration of time for Eq. (42), Eq. (43) can finally withdraw the standard deviation of the displacement response through the multiplication of the extraction vector $\boldsymbol{v}$ and its transpose. Typically, to withdraw the first diagonal element of matrix, $\boldsymbol{v}^{\mathrm{T}}$ can be defined as [1 0 ⋯ 0].

$$\sigma_u(t)=\sqrt{\int_{-\infty}^{+\infty}\boldsymbol{v}^{\mathrm{T}}\boldsymbol{S}_{uu}(\omega,\ t)\boldsymbol{v}\mathrm{d}\omega} \tag{43}$$

4 Case study

4.1 PSD parameters of random excitation

The seismic acceleration spectrum is centered on the remarkable frequency with a gentle peak, and then the intensity decreases as the frequency becomes higher. For the vertical seismic acceleration input, the white noise filter model suggested by KANAI and TAJIMI is adopted [25].

$$S_e(\omega)=\frac{1+4\xi_g^2\left(\dfrac{\omega}{\omega_g}\right)^2}{\left[1-\left(\dfrac{\omega}{\omega_g}\right)^2\right]^2+4\xi_g^2\left(\dfrac{\omega}{\omega_g}\right)^2}S_0 \tag{44}$$

The parameters of the subsoil filter model are different for different sites. The site Class I is considered, namely rock or compact gravel soil. The study is mainly divided into 3 cases, namely, no earthquake, weak earthquake and the intensive earthquake corresponding to the intensity of 0, 6 and 7, respectively. The relevant filter model parameters and the white noise spectrum value at each intensity are shown in Table 3.

Table 3 Parameter values of seismic acceleration PSD

Parameter	Value
Dominant ground frequency, ω_g/(rad·s^{-1})	25.13
Ground damping ratio, ξ_g	0.64
White spectrum S_0 at the seismic intensity of 0/(m^2·s^{-3})	0
White spectrum S_0 at the seismic intensity of 6/(m^2·s^{-3})	7.24×10^{-4}
White spectrum S_0 at the seismic intensity of 7/(m^2·s^{-3})	2.75×10^{-2}

The German vertical track irregularity PSD [26] is used, and can be expressed as:

$$S_v(n)=\frac{A_v n_c^2}{(n^2+n_r^2)(n^2+n_c^2)} \tag{45}$$

where A_v is the roughness coefficient; n_c and n_r are the cutoff angular wave numbers; at the low disturbance condition, the corresponding values are listed in Table 4.

Table 4 Values of vertical track irregularity PSD

Parameter	Value
Roughness coefficient, A_v/(m·rad)	4.032×10^{-7}
Cutoff angular wave number, n_r/(rad·m^{-1})	0.0206
Cutoff angular wave number, n_c/(rad·m^{-1})	0.8246

4.2 Parameters of TBS

The parameters in Table 5 of the high-speed train CRH2 are used for analysis, while the 32 m high-speed railway reinforced concrete beams in Table 6 are adopted for the analysis of the bridge whose natural frequency and linear density are respectively 6.6 Hz and 43 t/m.

To ensure the accuracy of the results, the train starts from a certain length of track irregularity to the bridge. The seismic acceleration is input to the bridge and the train simultaneously. According to ISO 2631 [27], the upper and lower limits of angular wave number are determined, and the parameters are shown in Table 7.

Table 5 Parameter values of train

Train subsystem parameter	Value
Car-body mass, m_c/kg	40000
Bogie mass, m_b/kg	3000
Wheel-set mass, m_w/kg	2000
Car-body inertia, I_c/(kg·m^2)	2×10^6
Bogie inertia, I_b/(kg·m^2)	3000
Primary suspension stiffness, k_1/(N·m^{-1})	1×10^6
Primary suspension damping, c_1/(N·s·m^{-1})	20000
Secondary suspension stiffness, k_2/(N·m^{-1})	2×10^5
Secondary suspension damping, c_2/(N·s·m^{-1})	10000
Semi-distance of wheel-sets, d_1/m	1.25
Semi-distance of bogies, d_2/m	8.75
Distance of vehicle, l_v/m	25
Train speed, V/(km·h^{-1})	360

Table 6 Parameter values of beam element

Bridge subsystem parameter	Value
Elastic modulus, E/Pa	3.55×10^{10}
Inertia, I/m^4	22.5
Section area, S/m^2	17.5
Material density, ρ/(kg·m^{-3})	2500
Beam element length, l_{be}/m	3.2
Damping ratio, ξ	0.02

Table 7 Parameter values of time and frequency

Parameter	Value
Lower limit of angular frequency, ω_{min}/rad	40π
Upper limit of angular frequency, ω_{max} /rad	π/100
Sampling rate of angular frequency, dω/rad	π/25
Lower limit of time, t_{min}/s	0
Upper limit of time, t_{max}/s	17
Time sampling rate, Δt/s	0.0025
Arrival instant on the bridge for the first wheel-set, t_0/s	$8l_v/V$
Lower limit of angular wave number, n_{min}/(rad·m^{-1})	π/40
Upper limit of angular wave number, n_{max}/(rad·m^{-1})	2π
Sampling rate of angular wave number, Δn/(rad·m^{-1})	π/400

4.3 Description of train crossing process

Each solution to TBS subjected to a random excitation time history sample containing the track irregularity and the seismic excitation is called once sampling of MCM which corresponds to once train-passing process, and generates a sample of the time history of bridge acceleration response, wheel-rail force, offload factor, etc.

The process when the 8-vehicle train crosses the bridge is divided into three stages as shown in Figure 3. Firstly, in Figure 3(a), to ensure the stability the solution to each vehicle element, the train starts from t_{min}=0 s at the initial distance that its first wheel-set is 8 times distance of vehicle (8×25= 200 m) away from the closest support. Simultaneously, the seismic excitation is input, in the form of displacement and velocity, to the wheel-set and in the form of acceleration to the support.

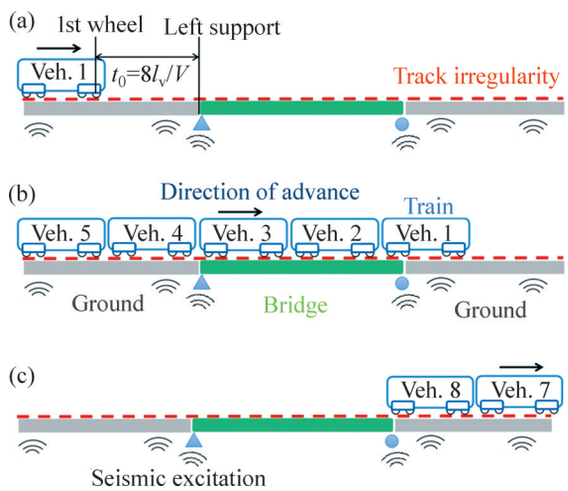

Figure 3 Schematic diagram of the train crossing the bridge: (a) The train comes close to the bridge; (b) The train crosses the bridge; (c) The train leaves the bridge

Secondly, in Figure 3(b), after the first wheel-set arrives at the closest support, which takes $8l_v/V$ seconds corresponding to t_0 in Table 7, the train begins to cross the bridge. The motion of the wheel-sets on the bridge is only coupled with the response of bridge and the track irregularity while the motion of the wheel-sets outside the bridge is only coupled with the seismic displacement and velocity and the track irregularity.

Thirdly, in Figure 3(c), when the last wheel-set leaves the farthest support and runs a certain distance, the process is terminated. The whole process will take 17 s, which can guarantee that the entire train can cross the bridge in different cases of speed from 90 to 720 km/h.

4.4 Analysis of precision and correctness

The train at a speed of 252 km/h is simulated to cross the bridge subjected to the earthquake at the intensity of 6. PEM-PIM and MCM-NβM are adopted respectively. A sampling result of acceleration and offload factor is respectively

plotted in Figures 4 and 6, while their statistic standard variance is plotted in Figures 5 and 7. The result shows that:

1) In Figure 4, the vertical acceleration response at the mid-span is comprehensively much smaller than that on the ground, which reflects that the stiffness and the mass of the bridge are much less than that of the ground.

2) In Figures 5 and 7, it takes longer time and a larger amount of samples for MCM-NβM, at least 10000 times, to reach as high as the solution precision by PEM-PIM, which reflects that PEM-PIM is highly precise and efficient, and the consistency of the standard variance curve by PEM-PIM and MCM-NβM demonstrates the correctness of programming procedure.

3) In Figure 6, the sub-graph represents the period where the first wheel-set moves on the bridge. By comparison of different combination of input, the influence from the seismic excitation on the offload factor is not obvious as for single sampling, while in Figure 7, the offload factor standard variance will highly peak when the wheel-set reaches the mid-span, which reflects that the random analysis method is of necessity and the sensitive and unsafe interval of offload factor is located on the bridge.

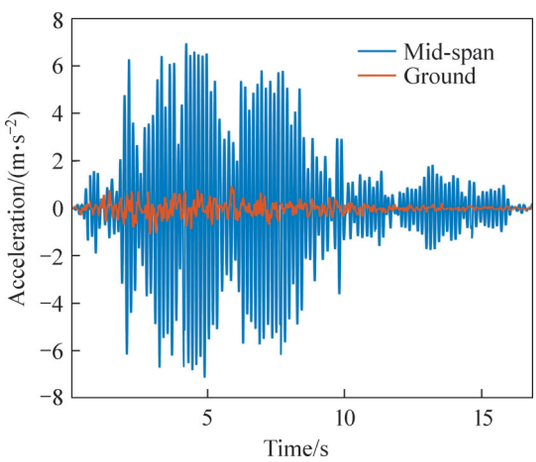

Figure 4 Comparison of two acceleration samples of MCM between at the mid-span and on the ground

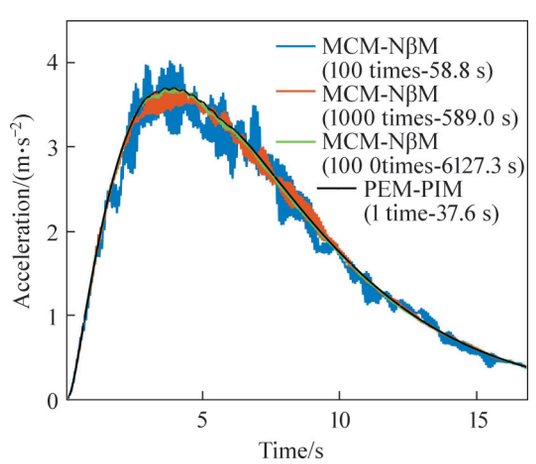

Figure 5 Comparison of the precision and efficiency of the acceleration standard variance at mid-span between PEM-PIM and MCM-NβM

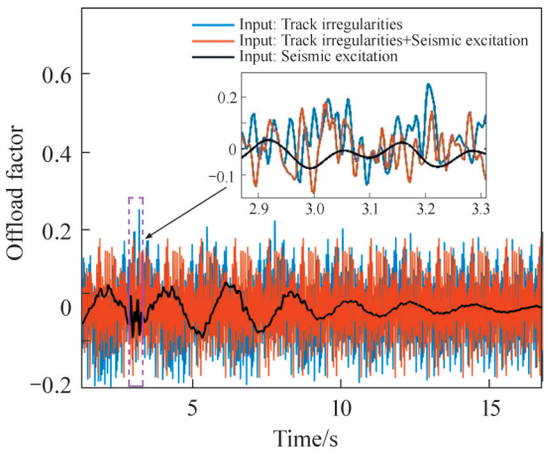

Figure 6 Comparison of an offload sample of MCM in different conditions of random excitation

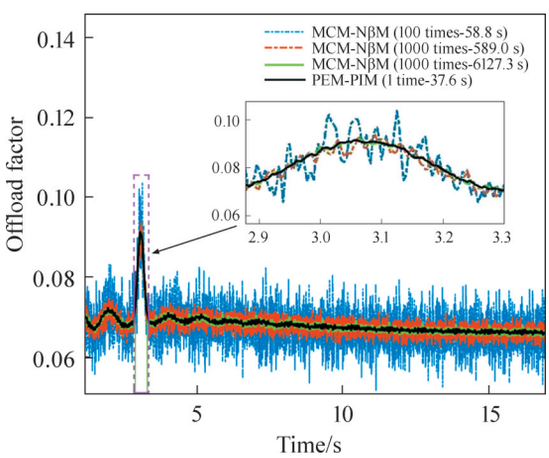

Figure 7 Comparison of the precision of the offload factor standard variance for the first wheel-set between PEM-PIM and MCM-NβM

4.5 Analysis of bridge acceleration EPSD

By PEM-PIM, the train at a speed of 252 km/h is simulated to cross the bridge subjected to the earthquake respectively at the intensity of 0, 6 and 7. The EPSD of mid-span vertical acceleration is shown in Figure 8. The result shows that:

1) The EPSD of the vertical acceleration at the

mid-span of the bridge only subjected to the track irregularity, namely without seismic excitation shown in Figure 8(a), has a wider frequency band than the ones subjected to the earthquake at the intensity of 6 and 7 shown in Figures 8(b) and (c), and contains the dominant components at the high frequency interval from 50 to 60 Hz.

2) For the bridge under the earthquake shown in Figures 8(b) and (c), the EPSD of the vertical acceleration at mid-span contains the dominant components closer to 6.6 Hz, the natural frequency of the bridge, and has the highest order of 10^2 at the seismic intensity of 7.

3) In general, the intensive earthquake has the greatest impact on the bridge so that the influence from the track irregularity can be neglected. The dominant frequency of the bridge vertical acceleration response locates in the natural frequency of the bridge.

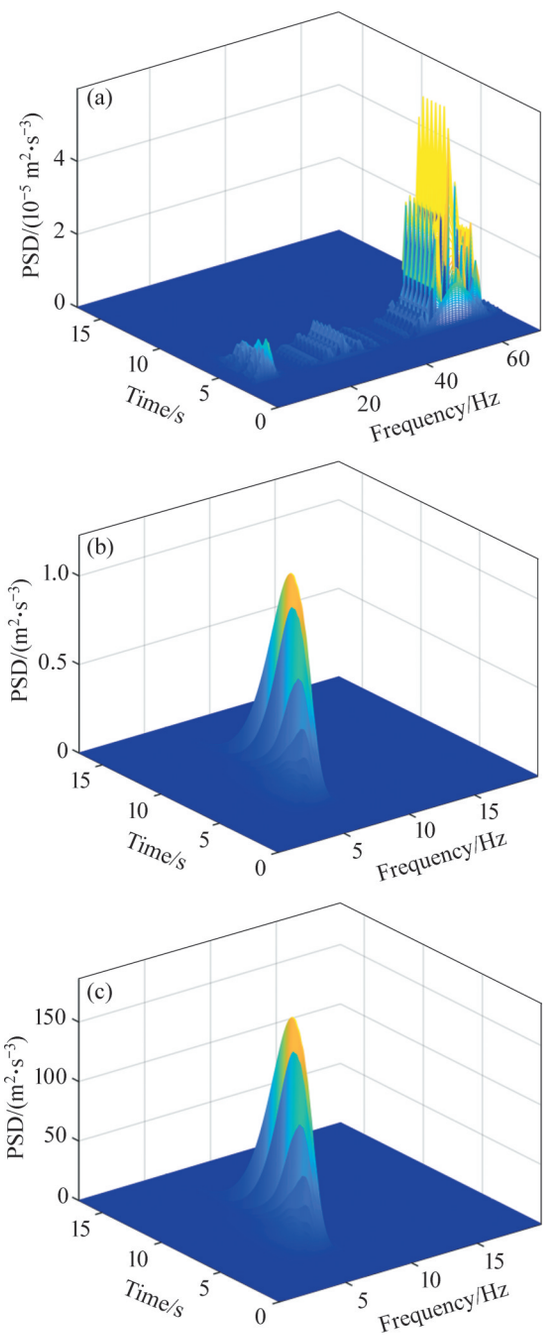

Figure 8 EPSD of the mid-span vertical acceleration: (a) Bridge under the seismic intensity of 0; (b) Bridge under the seismic intensity of 6; (c) Bridge under the seismic intensity of 7

4.6 Analysis of bridge acceleration distribution histories

By MCM-NβM (1000 samples), the train at a speed of 252km/h is simulated to cross the bridge subjected to the earthquake respectively at the intensity of 0, 6 and 7. The GOF histories, the distribution histories of the mid-span vertical acceleration and possibility density function (PDF) curves at mid-span are respectively shown in Figures 9−11. The results show that:

1) In Figure 9, the GOF histories are larger than 0.99, and in Figure 11, the tentative and theoretical PDF curve graphically share a high fitting degree at a certain instant, which means the samples of vertical acceleration at mid-span obeys the normal distribution at any instant. However, at the seismic intensity of 0, before the train runs on the bridge, the randomness of the bridge response does not exist, neither does goodness of fit during this period.

2) In Figures 10(a), (b) and (c), most of acceleration samples by MCM-NβM are

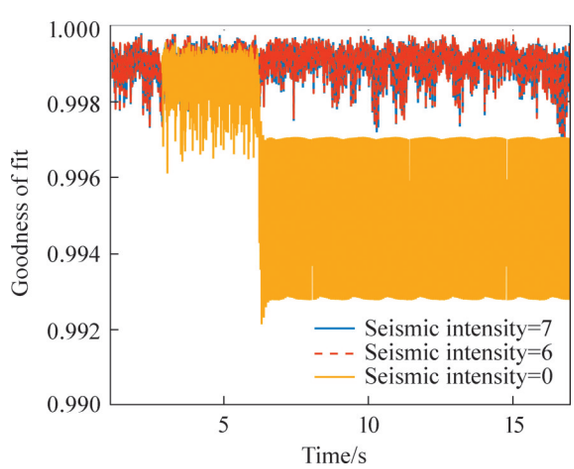

Figure 9 GOF histories between the tentative and the theoretical normal distribution of the mid-span vertical acceleration at different seismic intensities

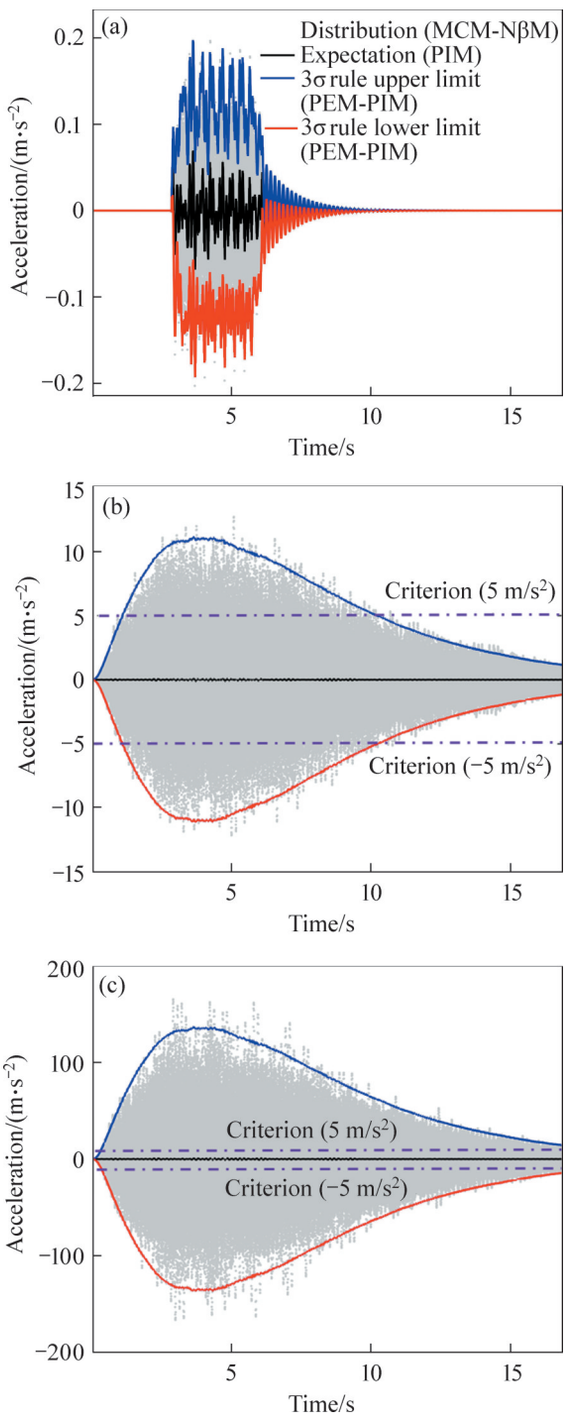

Figure 10 Distribution histories of the mid-span vertical acceleration: (a) Bridge at the seismic intensity of 0; (b) Bridge at the seismic intensity of 6; (c) Bridge at the seismic intensity of 7

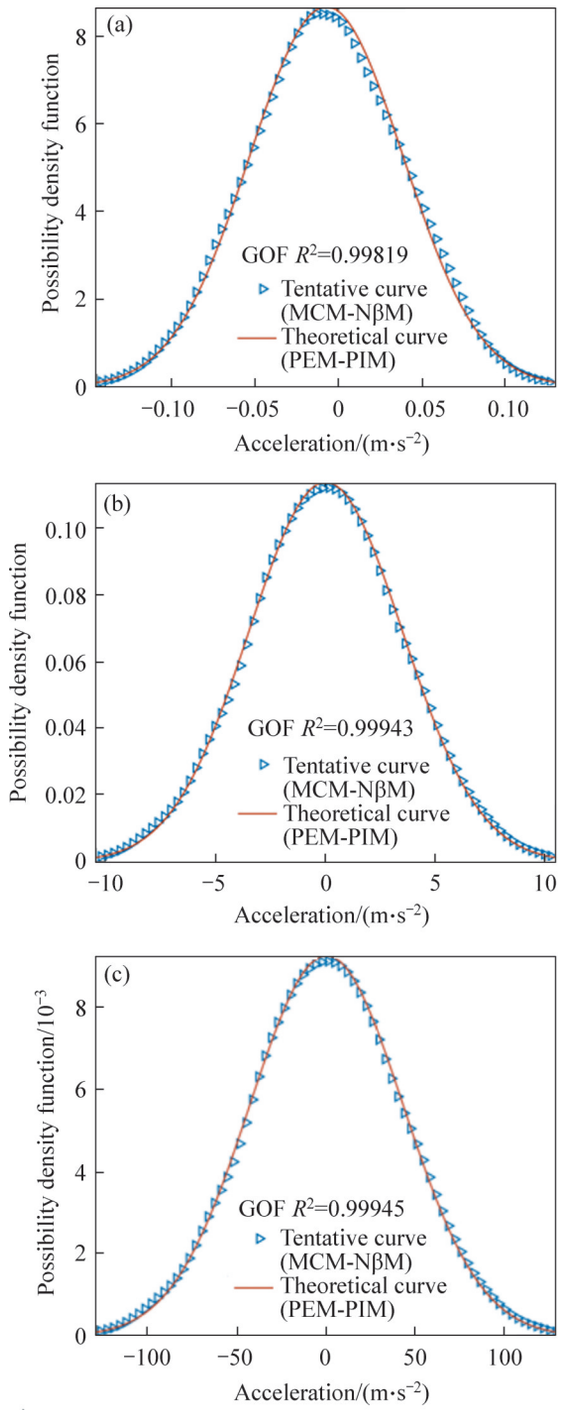

Figure 11 PDF curve of the mid-span vertical acceleration: (a) Bridge at the seismic intensity of 0; (b) Bridge at the seismic intensity of 6; (c) Bridge at the seismic intensity of 7

symmetrically distributed within the range of 3σ principle by PEM-PIM and their expectation locates on the zero line. According to the statistics, the over-limit possibility of the vertical acceleration at the seismic intensity of 0, 6 and 7 are respectively 0%, 13.7% and 97.3%.

3) In general, the bridge acceleration response under the intensive earthquake is a non-stationary zero-mean Gaussian random process whose distribution limit can be determined by 3σ principle, and probably, the intensive earthquake has an extremely harmful effect on the bridge.

4.7 Analysis of wheel-rail force EPSD

Under the same studied case as Section 4.5, since the offload factor is related to wheel-rail force, the EPSD of wheel-rail force is analyzed and shown in Figure 12. The result shows that:

1) The EPSD of the vertical wheel-rail force on the bridge only subjected to the track irregularity, namely without seismic excitation shown in Figure 12(a), has a wider time and frequency band than the ones subjected to the earthquake at the intensity of 6 and 7 shown in Figures 12(b) and (c), and almost keeps constant along the time axis.

2) For the bridge under the earthquake, the EPSD of the vertical wheel-rail force contains the dominant components closer to 6.6 Hz, the natural frequency of the bridge, and meanwhile reaches, at a certain moment, a sudden peak which has the highest order of 10^8 at the seismic intensity of 7. By comparison with the case only subjected to the track irregularity in Figure 12(a), the sudden peak in the EPSD of the vertical wheel-rail force for Figures 12(b) and (c) results from the application of seismic excitation.

3) In general, when the earthquake does not occur, the wheel-rail force is a stationary process. The intensive earthquake will, in time domain, lend to the surge of wheel-rail force dominated by the component of the natural frequency of bridge, while the weak one will have less influence on the wheel-rail force.

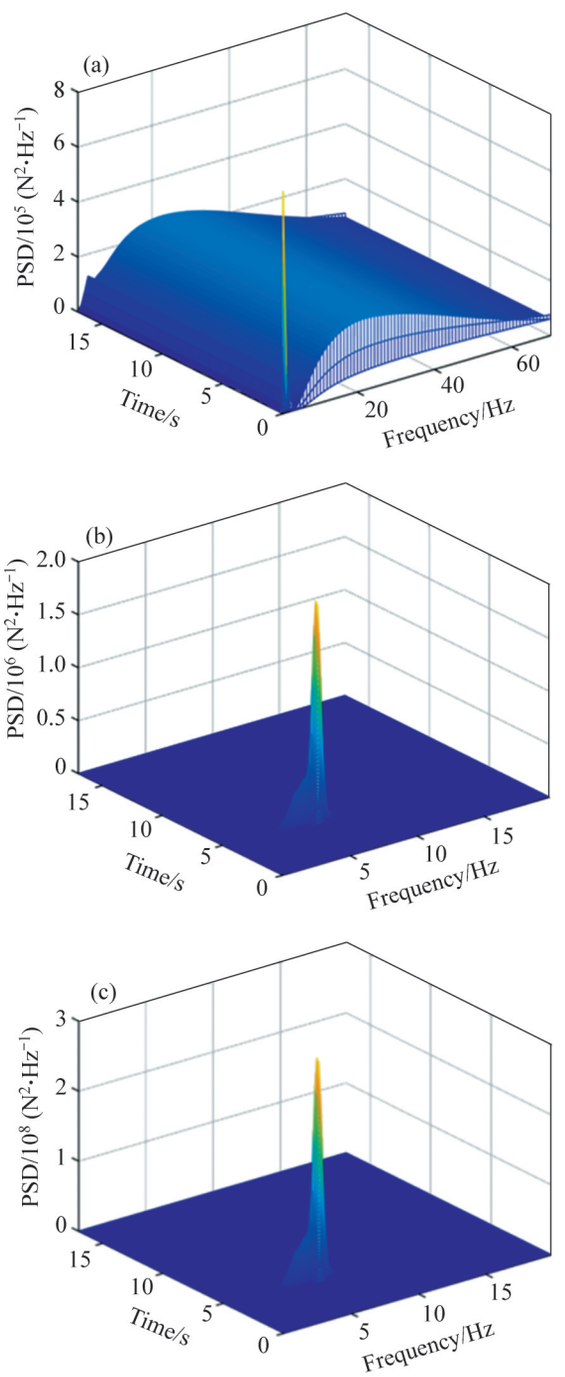

Figure 12 EPSD of the wheel-rail force: (a) Bridge at the seismic intensity of 0; (b) Bridge at the seismic intensity of 6; (c) Bridge at the seismic intensity of 7

4.8 Analysis of time history distribution of offload factor

Under the same studied case as Section 4.6, the GOF histories, the distribution histories of the offload factor and PDF curve are respectively shown in Figures 13−15. The results show that:

1) In Figure 13, the GOF of tentative and theoretical PDF curve is larger than 0.99, and in Figure 15, the tentative and theoretical PDF curve share a high fitting degree at a certain instant, which means the samples of offload factor obey the normal

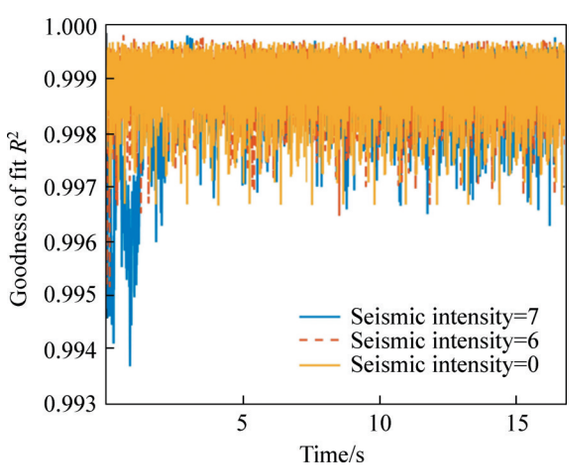

Figure 13 GOF histories between the tentative and the theoretical normal distribution of the offload factor at different seismic intensities

distribution at any instant.

2) In Figures 14(a), (b) and (c), most of offload factor samples by MCM-NβM are symmetrically distributed within the range of 3σ principle by PEM-PIM and their expectation locates on the zero line. At certain range of time, the distribution of offload factor has a surge, and according to the statistics, its over-limit possibility at the seismic intensity of 0, 6 and 7 are respectively 0%, 0% and 42.7%. The negative value of offload factor means that the wheel-set is on-loading and it is safe for the train to cross the bridge. At the seismic intensity of 7, the offload factor distribution has the highest 3σ upper limit.

3) In general, the offload factor under the intensive earthquake is a weakly stationary zero-

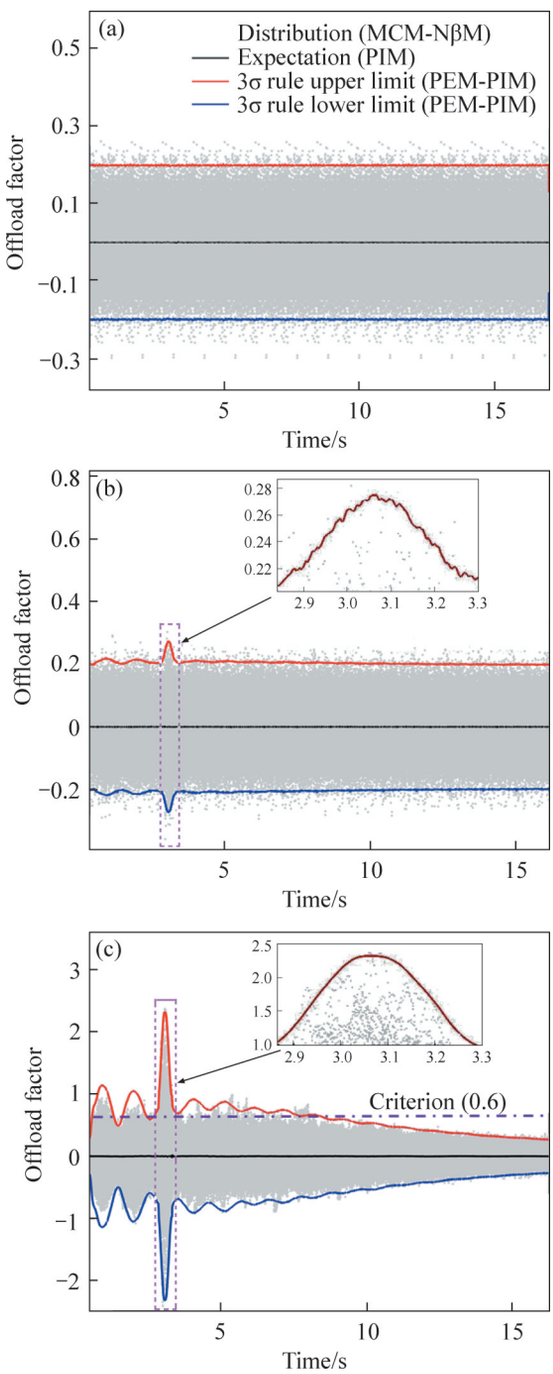

Figure 14 Distribution histories of the offload factor: (a) Bridge at the seismic intensity of 0; (b) Bridge at the seismic intensity of 6; (c) Bridge at the seismic intensity of 7

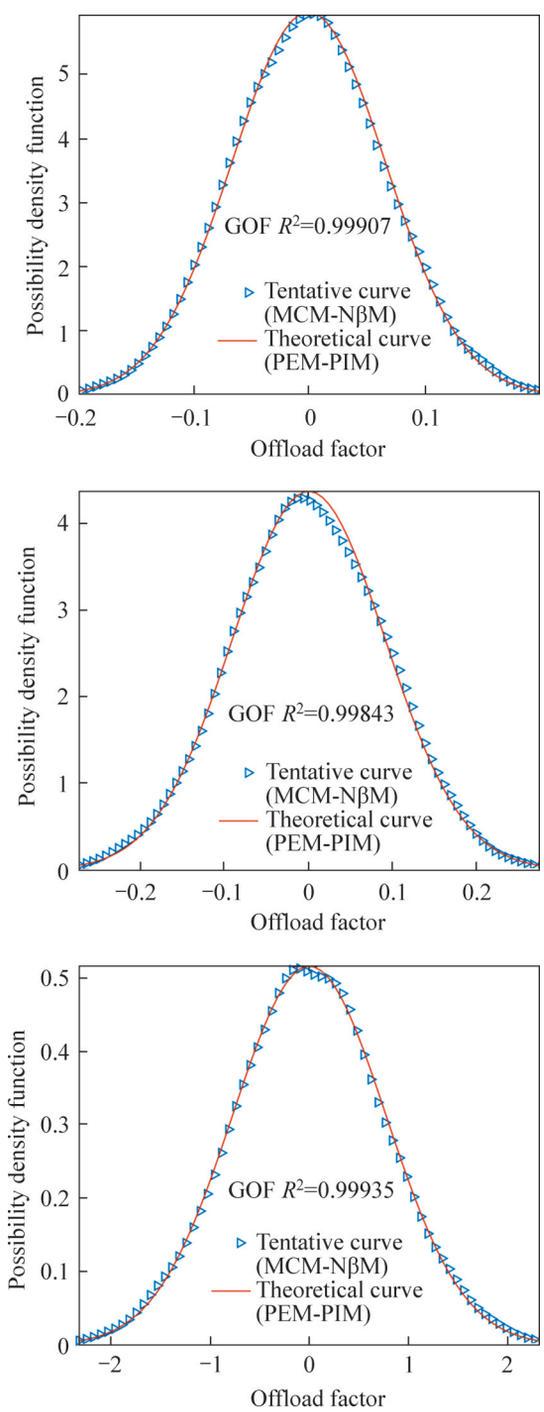

Figure 15 PDF curves of the offload factor: (a) Bridge at the seismic intensity of 0; (b) Bridge at the seismic intensity of 6; (c) Bridge at the seismic intensity of 7

mean Gaussian random process whose distribution limit can be determined by 3σ principle, and probably, the intensive earthquake will lead to the unsafe passage of the train on the bridge.

4.9 Analysis of the relation between the offload factor and the train speed

For the analysis of the offload factor as the function of the train speed, PEM-PIM is adopted and the offload factor peak curve of 3σ principle is analyzed at the speed from 90 to 720 km/h with the bandwidth of 9 km/h and shown in Figure 16. Also, statistics of the speed for the offload factor peak appearing on the bridge at different seismic intensities is shown in Figure 17. The results show that:

1) In Figure 16, at the seismic intensity of 0 and 6, the offload factor peak increases with the increase of train speed and presents a quadratic linear relationship with the train speed. The tendency of offload factor peak-speed curves is close to each other and almost shares the same speed limit of 400 km/h at the criterion line. Under this circumstance, the bridge response contributes weakly to the offload factor, and the influence from the track irregularity velocity and acceleration containing the factors of V and V^2, namely train speed and its square, accounts for the quadratic linear relationship. At the the seismic intensity of 7, the overall offload factor peak-speed curve exceeds the criterion line. Its tendency fluctuates with the increase of speed.

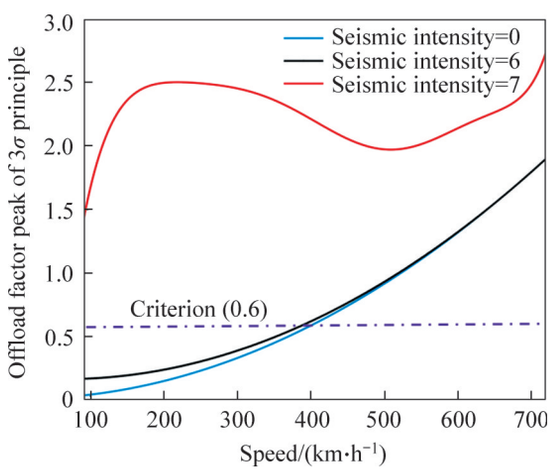

Figure 16 Relation curve between offload factor peak of 3σ principle and train speed

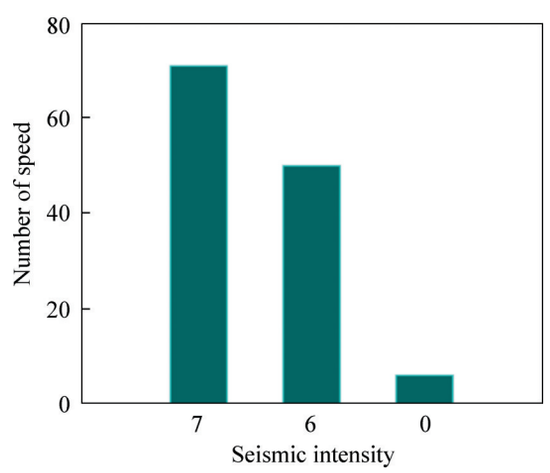

Figure 17 Statistics of the speed cases for the offload factor peak appearing on the bridge at different seismic intensities

2) In Figure 17, for all the speed cases (71 cases of speed), the offload factor peak can only be found when the wheel-set is on the bridge at the seismic intensity of 7, which demonstrates that the bridge response will be so largely influenced by the intensive earthquake that it has the main impact on the offload factor. Under the intensive earthquake, the train speed contributes weakly to the offload factor.

3) In general, the offload factor is positively correlated with train speed in the condition of weak earthquake. The weak earthquake pose less threat to the passage of train on the bridge, which means, by strictly controlling the train speed, the safe passage on the bridge can be guaranteed, while for the intensive earthquake, the passage of train is completely unsafe and halting the operation of train is highly recommended.

5 Conclusions

1) It is feasible to study TBS under intensive earthquakes based on the random vibration method. Compared with the seismic acceleration using only a single sample, MCM based on multiple samples is more statistically accurate, and based on the input-output PSD conversion process, PEM is more efficient and accurate.

2) Adopting time-derivable slow-varying uniform modulation function to separate the stationary and non-stationary part of random excitation is workable and can well preserve the time domain characteristics of the random process.

3) The bridge acceleration and offload factor under the intensive earthquake is respectively non-

stationary and weakly stationary zero-mean Gaussian random process whose distribution limit can be determined by 3σ principle.

4) Under the weak earthquake, the train speed has the main impact on the offload factor, while the bridge response contributes weakly to the offload factor. At the intensive earthquake, the train speed contributes weakly to the offload factor, while the bridge contributes to the offload factor the most. The intensive earthquake will probably have an extremely harmful effect on the bridge and pose threat to the passage of train on the bridge. Under the circumstance, the passage of train is completely unsafe and halting the operation of train is highly recommended.

Contributors

WU Zhao-zhi came up with the concept, realized the simulation, analyzed the data and edited the draft of manuscript. ZHANG Nan conducted the literature review, checked the computations, wrote the draft of the manuscript replied to reviewers' comments and revised the final version.

Conflict of interest

The authors declare that they have no known competing financial interests or personal relationships that could have appeared to influence the work reported in this paper.

Reference

[1] O'REILLY G J. Seismic intensity measures for risk assessment of bridges [J]. Bulletin of Earthquake Engineering, 2021, 19(9): 3671−3699. DOI: 10.1007/s10518-021-01114-z.

[2] YAU J D, FRÝBA L. Response of suspended beams due to moving loads and vertical seismic ground excitations [J]. Engineering Structures, 2007, 29(12): 3255 − 3262. DOI: 10.1016/j.engstruct.2007.10.001.

[3] YAU J D. Dynamic response analysis of suspended beams subjected to moving vehicles and multiple support excitations [J]. Journal of Sound and Vibration, 2009, 325(4−5): 907−922. DOI: 10.1016/j.jsv.2009.04.013.

[4] NISHIMURA K, TERUMICHI Y, MORIMURA T, et al. Experimental study on the vehicle safety by earthquake track excitation with 1/10 scale vehicle and roller rig [J]. Journal of System Design and Dynamics, 2010, 4(1): 226−238. DOI: 10.1299/jsdd.4.226.

[5] NISHIMURA K, TERUMICHI Y, MORIMURA T, et al. Analytical study on the safety of high speed railway vehicle on excited tracks [J]. Journal of System Design and Dynamics, 2010, 4(1): 211−225. DOI: 10.1299/jsdd.4.211.

[6] HE Xing-wen, KAWATANI M, HAYASHIKAWA T, et al. Numerical analysis on seismic response of Shinkansen bridge-train interaction system under moderate earthquakes [J]. Earthquake Engineering and Engineering Vibration, 2011, 10(1): 85−97. DOI: 10.1007/s11803-011-0049-1.

[7] LOH C H, LEE Zheng-kuan. Seismic monitoring of a bridge: Assessing dynamic characteristics from both weak and strong ground excitations [J]. Earthquake Engineering & Structural Dynamics, 1997, 26(2): 269 − 288. DOI: 10.1002/(SICI)1096-9845(199702)26: 2<269: AID-EQE644>3.0.CO;2-H.

[8] QI Jing-jing, JIANG Li-zhong. Experimental study on seismic behaviors of steel-concrete composite frames [J]. Journal of Central South University, 2015, 22(11): 4396 − 4413. DOI: 10.1007/s11771-015-2988-6.

[9] ZHU Zhi-hui, GONG Wei, WANG Kun, et al. Dynamic effect of heavy-haul train on seismic response of railway cable-stayed bridge [J]. Journal of Central South University, 2020, 27(7): 1939−1955. DOI: 10.1007/s11771-020-4421-z.

[10] LIN Jia-hao, ZHANG Wen-shou, WILLIAMS F W. Pseudo-excitation algorithm for nonstationary random seismic responses [J]. Engineering Structures, 1994, 16(4): 270−276. DOI: 10.1016/0141-0296(94)90067-1.

[11] ZHANG Z C, LIN J H, ZHANG Y H, et al. Nonstationary random vibration analysis of coupled vehicle-bridge systems [J]. Engineering Computations, 2010, 27(6): 712−732. DOI: 10.1108/02644401011062108.

[12] HE Xu-hui, SHI Kang, WU Teng. An efficient analysis framework for high-speed train-bridge coupled vibration under non-stationary winds [J]. Structure and Infrastructure Engineering, 2020, 16(9): 1326 − 1346. DOI: 10.1080/15732479.2019.1704800.

[13] ZHU Si-yu, LI Yong-le. Random characteristics of vehicle-bridge system vibration by an optimized pseudo excitation method [J]. International Journal of Structural Stability and Dynamics, 2020, 20(5): 2050069. DOI: 10.1142/s0219455420500698.

[14] YU He-lu, WANG Bin, XIA Cui-peng, et al. Efficient non-stationary random vibration analysis of vehicle-bridge system based on an improved explicit time-domain method [J]. Engineering Structures, 2021, 231: 111786. DOI: 10.1016/j.engstruct.2020.111786.

[15] XIA He, ZHANG Nan, GUO Wei-wei. Dynamic interaction of train-bridge systems in high-speed railways [M]. Berlin, Heidelberg: Springer Berlin Heidelberg, 2018. DOI: 10.1007/978-3-662-54871-4.

[16] BATHE K J. Finite element procedures [M]. Prentice Hall, Pearson Education, Inc, 2006.

[17] ARGENTINI T, PAGANI A, ROCCHI D, et al. Monte Carlo analysis of total damping and flutter speed of a long span bridge: Effects of structural and aerodynamic uncertainties [J]. Journal of Wind Engineering and Industrial Aerodynamics, 2014, 128: 90 − 104. DOI: 10.1016/j. jweia. 2014.02.010.

[18] BOGDANOFF J L, GOLDBERG J E, BERNARD M C. Response of a simple structure to a random earthquake-type disturbance [J]. Bulletin of the Seismological Society of America, 1961, 51(2): 293 − 310. DOI: 10.1785/bssa051002

0293.
[19] LIN J H, ZHANG Y H, LI Q S, et al. Seismic spatial effects for long-span bridges, using the pseudo excitation method [J]. Engineering Structures, 2004, 26(9): 1207–1216. DOI: 10.1016/j.engstruct.2004.03.019.
[20] ZHONG Wan-xie, CAI Zhi-qin. Precise integration method for LQG optimal measurement feedback control problem [J]. Applied Mathematics and Mechanics, 2000, 21(12): 1417–1422. DOI: 10.1007/BF02459220.
[21] TB10621—2014. Code for design of high-speed railway [S]. China Railway Publishing House. (in Chinese)
[22] ZHANG Nan, XIA He. A vehicle-bridge interaction dynamic system analysis method based on inter-system iteration [J]. China Railway Science, 2013, 34(5): 32−38. (in Chinese)
[23] HOROVÁ I, KOLÁČEK J, ZELINKA J. Kernel smoothing in Matlab [M]. Singapore: World Scientific, 2012. DOI: 10.1142/8468.
[24] ZGHOUL A A. A goodness of fit test for normality based on the empirical moment generating function [J]. Communications in Statistics-Simulation and Computation, 2010, 39(6): 1292 – 1304. DOI: 10.1080/03610918.2010.490318.
[25] ROFOOEI F R, MOBARAKE A, AHMADI G. Generation of artificial earthquake records with a nonstationary Kanai-Tajimi model [J]. Engineering Structures, 2001, 23(7): 827–837. DOI: 10.1016/S0141-0296(00)00093-6.
[26] XIANG Jun, LI De-jian, ZENG Qing-yuan. Simulation of spatially coupling dynamic response of train-track time-variant system [J]. Journal of Central South University of Technology, 2003, 10(3): 226–230. DOI: 10.1007/s11771-003-0014-x.
[27] LIU Chi, THOMPSON D, GRIFFIN M J, et al. Effect of train speed and track geometry on the ride comfort in high-speed railways based on ISO 2631-1 [J]. Proceedings of the Institution of Mechanical Engineers, Part F: Journal of Rail and Rapid Transit, 2020, 234(7): 765–778. DOI: 10.1177/0954409719868050.

(Edited by HE Yun-bin)

中文导读

基于随机振动方法的强震作用下车桥耦合系统动力响应研究

摘要：地震荷载是自然界中一种突发并且对结构具有一定破坏性的随机激励。当震级大于6级即地震烈度在7以上的地震即强震作用在车桥耦合系统中时，确定系统响应的概率分布特性用于保障行车和结构安全稳定十分重要。因此，本文分别采用蒙特卡洛实验法以及虚拟激励随机振动分析方法，构建二维车桥耦合系统空间状态方程，考虑轨道不平顺随机激励和确定性轴重激励，以及通过大质量法输入地震随机激励，借助精细积分法通过全过程迭代过程对该状态方程进行精确高效求解响应时程分布。由此确定系统响应及相应动力学指标的概率分布，与非强震条件下的响应概率分布特性对比，最终为保障行车和桥梁结构安全稳定提供建议。

关键词：随机振动方法；强震；车桥耦合系统；概率分布；空间状态方程；全程迭代法；精细积分